RESEARCH ON PROPERTIES OF MOLTEN BASALT

CONTENTS

1.	**Preparation of a basalt feed sample for analysis**	**1**
2.	**Analysis of basalt feed**	**1**
3.	**Thermal properties**	**5**
4.	**Phase analysis of basalt samples**	**7**
5.	**Definition of a structural coordination state of iron cations**	**18**
6.	**Summary**	**26**

1. Preparation of a basalt bath sample for analysis

For research of basalt the initially obtained bath was thoroughly mixed. Thereafter a few samples were chosen, the combination of which resulted in an average sample. The samples were extracted from two different locations: from the surface and from the lower part of basalt feed. Obtained samples of rock were crushed and then ground up in a mill into fine powder.

2. Chemical analysis of basalt bath

The composition of a basalt rock sample was defined by the means of X-ray fluorescence analysis. The device used for X-ray fluorescence analysis of basalt was Axios Advanced by PANanalytical. An X-ray tube with Rh-anode with 4 kW capacity served as excitation source for characteristic emission. The measurements were made in vacuum of approx. 3 Pa. For testing the ground samples were pressed to tablets with polystyrol at the ratio of 1:12. The total amount of iron is represented as Fe_2O_3. The margin of error was ±0.1%.

Chart 1. Composition of samples, mass percent

Sample	SiO_2	Al_2O_3	TiO_2	Fe_2O_3	CaO	MgO	K_2O	Na_2O
Basalt	44.4	15.3	2.3	10.4	10.4	10.9	2.0	4.3

The chemical analysis of samples was carried out by the means of a scanning electron microscope JSM5910LV (JEOL Serving Advance Technology) and an energy-dispersing X-ray microanalyzer with

Crystal attachment (manufactured by Oxford Instrument Analytical). The accelerating of electron projector used was 20 kV; the magnification - from x1500 upwards. Prior to analysis a layer of gold has been sprayed onto the surface of samples by means of thermal evaporation on the Scancoat device (Edwards, UK).

The SEM-images obtained from the surface of the basalt rock sample are presented at Figure 1. According to these data, the feed has a microheterogenous composition; visible light and dark areas differ essentially in composition (Chart 2).

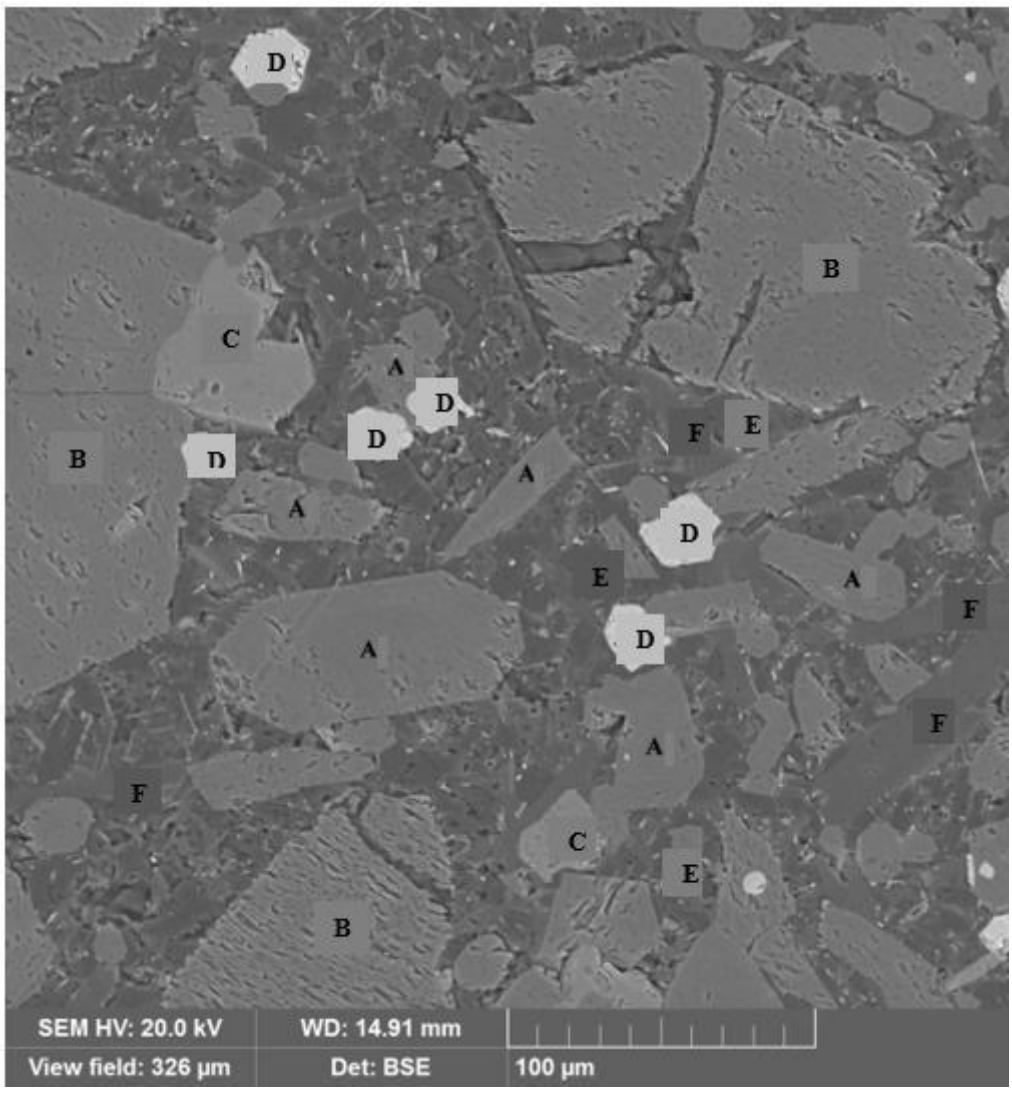

Fig. 1. Images of the initial basalt feed

The composition of available phases was defined by means of EDX analysis. The average values based on five measurements conducted for each sample are presented in Table 2. The letters on Picture 1 indicate the testing points on a basalt sample. Picture 2 shows the scaled-up testing points of analysis. The data in Chart 2 verify that the composition of basalt noticeably differs even within one single piece of rock.

Chart 2. Results of EDX analysis in chosen points of surface, mass percent

Point	SiO_2	Al_2O_3	TiO_2	Fe_2O_3	CaO	MgO	K_2O	Na_2O	MnO_2
A	49.1	5.9	2.3	6.9	21.4	13.8	-	0.5	-
B	50.4	20.1	-	18.8	1.5	7.3	-	1.2	-
C	25.8	16.7	9.2	23.4	11.1	12.6	-	1.3	-
D	-	8.3	16.1	70.7	-	4.0	-	-	0.9
E	52.1	27.3	-	1.1	0.4	-	3.6	15.5	-
F	54.1	29.2	-	0.6	11.2	-	0.5	4.5	-

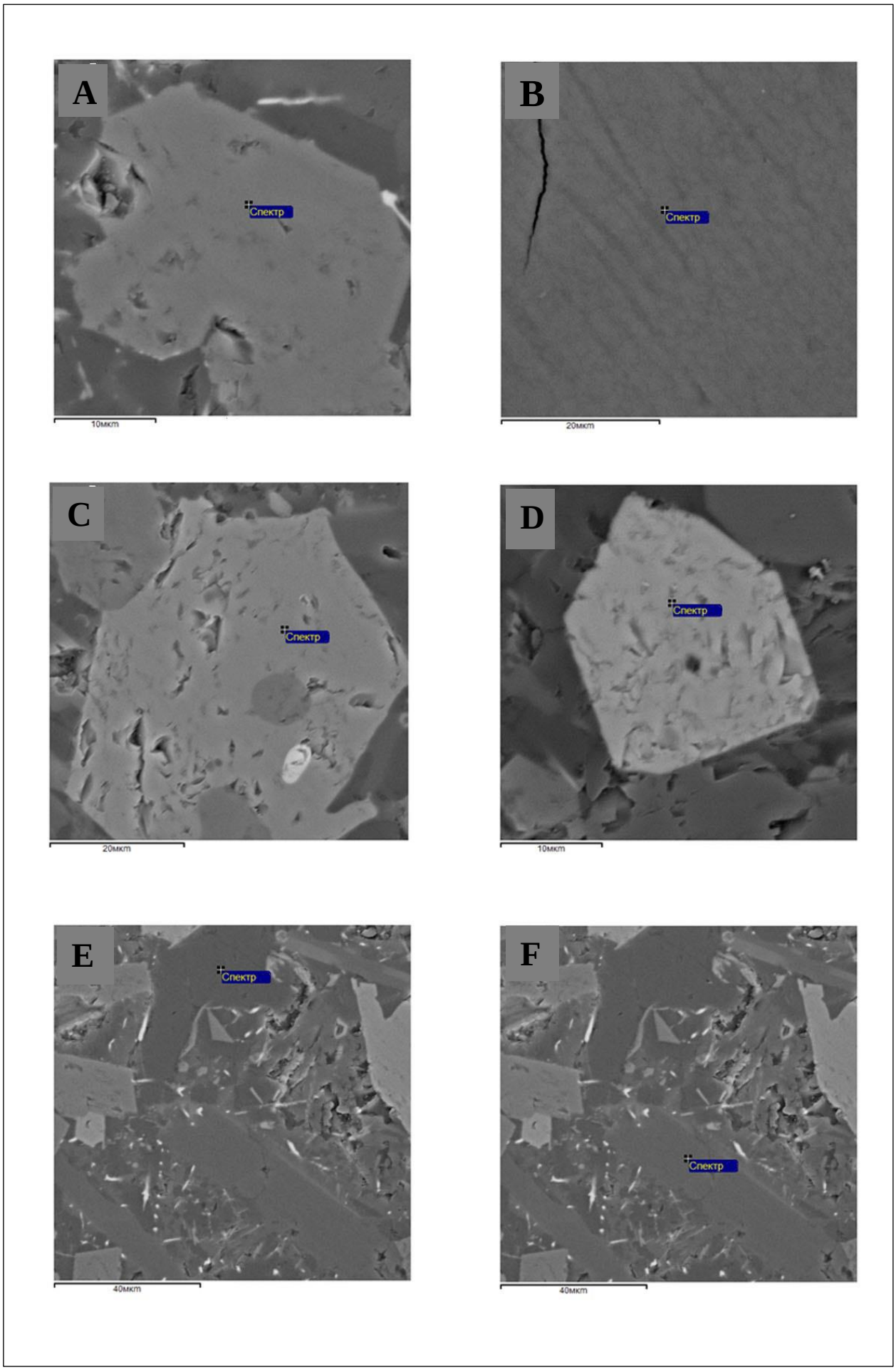

Fig. 2. SEM images of the various sampling points of basalt rock shear

2. Thermal properties

Thermal analysis of the original basalt rock was conducted by means of a synchronous thermal analyser STA Jupiter 449C by NETZSCH with a high-temperature furnace (operating t° = 20-1500 °C). A supersensitive sample holder with Pt/Pt-Rh thermocouples was used for testing. Platinum pots (working pot and comparison pot) were used in the experiment. During the testing the samples have been heated up at the speed of 10 °C/min from 20 to 1450 °C; the cooling followed by crystallization was conducted at the speed of 2 °C/min. For the purpose of higher precision of tests, a line of reference with two empty pots was imaged. The imaging of sample in the working pot was made in relation to the mentioned line of reference. The mass of the initial subsample amounted to ~83.5 mg. Method error of the temperature evaluation was ±2 °C.

Basalt is a natural mineral; it contains components which include hydroxides and carbonates. The presence of such thermally unstable compounds was confirmed by the data of thermal analysis. The heating curve DSC shows several endothermic effects at the temperatures of approx. 175, 507 и 628 °C, which are related to the moisture debinding and the disintegration of magnesium carbonate and calcium carbonate (Figure 3). The temperature of complete melting of a basalt sample is1176^{o}C. The beginning of melting is marked by a slight peak at 1050^{o}C. The thermogravimetric curve in the interval 25-1000°C shows a gradual decrease of mass (Figure 4). During cooling the rate of temperature change is lower, the thermal effects are substantially slighter, whereas two peaks of crystallization at 1085 и 1110°C were observed. Above the melting point the sample is in liquid state, and the temperature dependence of its heat capacity differs from that in the crystalline state. For this reason, the slope of DSC curve is being measured after melting.

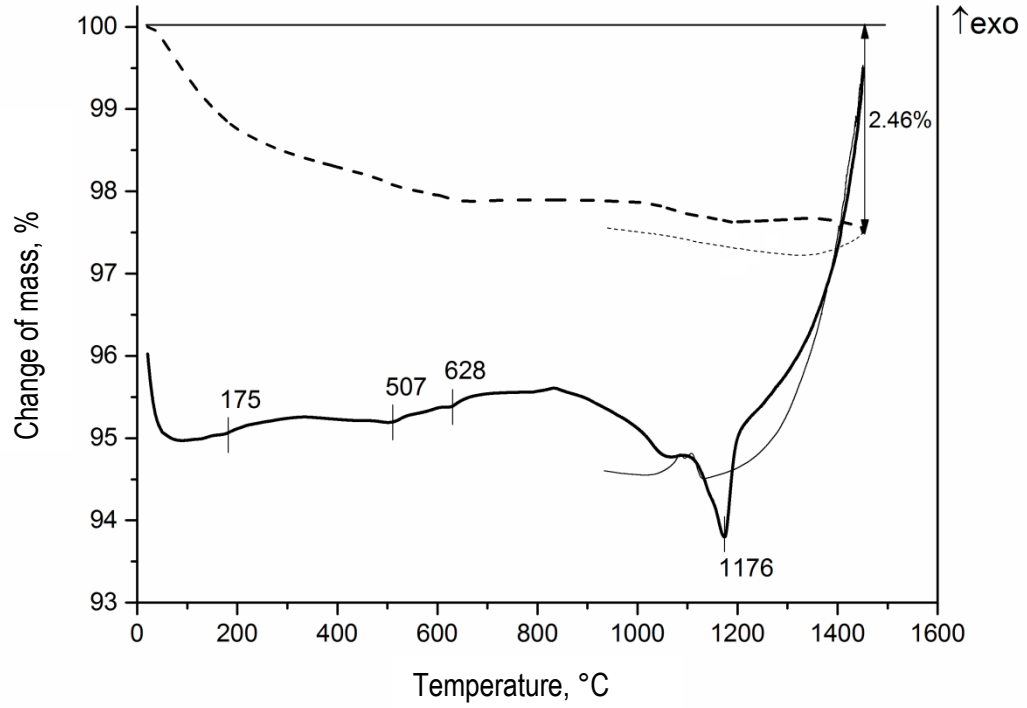

Fig. 3. Heating curves DSC (solid lines) и thermogravimetric (dashed lines) of basalt feed, obtained in air at the heating speed of 10°C/min

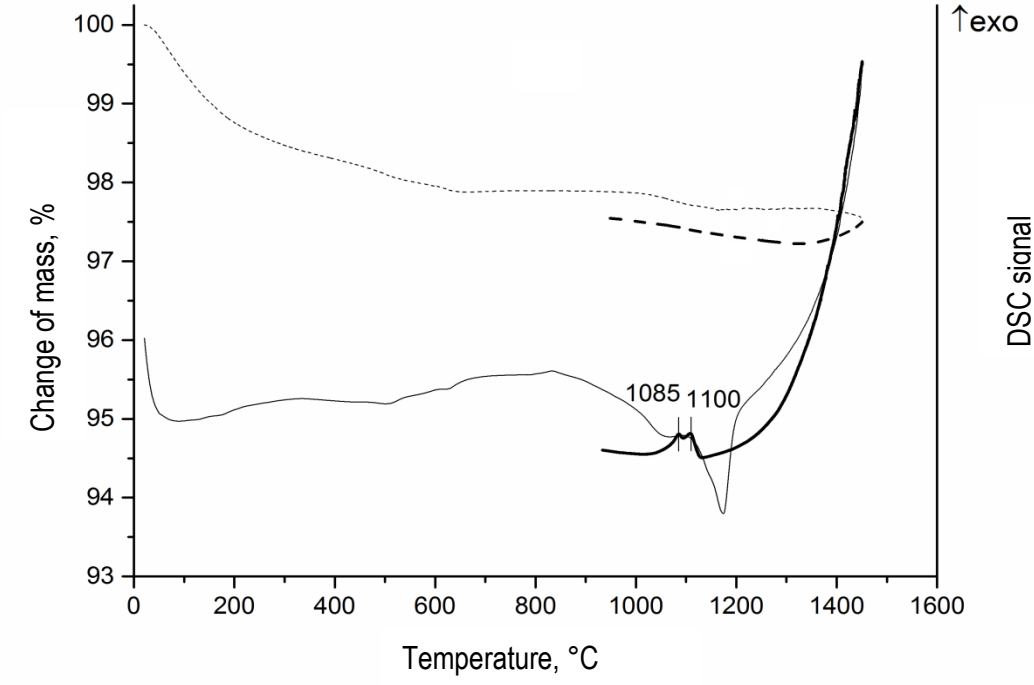

Fig. 4. Cooling curves DSC (solid lines) и thermogravimetric (dashed lines) of basalt feed, obtained in air at the heating speed of 10°C/min

4. Phase analysis of basalt samples

4.1. The aim of testing:

An X-ray analysis of the phase composition of polycrystalline samples of basalt and samples of an average basalt exposed to various temperatures (1000, 1100, 1200 и 1300°C) for 1 hour and water-hardened at the respective temperatures. To prevent an interaction of basalt samples with the material of the pot, the samples were annealed in platinum pots.

4.2. Equipment:

The analysis of the phase composition of samples was carried out on the basis of X-ray charts obtained at the X-ray powder diffractometer Thermo ARL X-TRA (reflection geometry (Bregg-Brentano), CuK_α emission, λ = 1.5418 Å, semiconductor Peltier detector). The X-ray charts of the detectors were obtained at room temperature between the angles 5°-70° 2θ and the recording speed 0.2°/min.

The X-ray charts were processed using the Powder Diffraction File database of the International Centre for Diffraction Data (ICDD).

The Rietveld method was applied for the quantitative phase analysis in the programme RIETAN97. The structural characteristics for specific phases were retrieved from the JCSD (International Crystal Structure Data Base). At defining the quantitative phase composition of the samples, the profile functions have been specified along with the parameters of located phases. The available phases of various structural types were localized in all samples (Pic. 1-8):

1) Phases with augite structure, $[(Mg,Ca,Fe)_2(Si_2O_6)]$, (http://www.mindat.org/min-419.html) antiferromagnetic, pyroxene family with general formula $(Ca,Na)(Mg,Fe^{2+},Al,Fe^{3+},Ti)[($ $K(Al_4Si_2O_9(OH)_3$, belonging to the group of layered silicates (http://www.mindat.org/min-2011.html), mica series, de facto representing K-deficient muscovite.
2) Phases with kaolinite 1A structure, $Al_2(Si_2O_5)(OH)_4)$, kaolinite-serpentine group (http://www.mindat.org/min-2156.html).
3) Silicon oxides: tridymite O, SiO_2, quartz, SiO_2, cristobalite low, SiO_2.
4) Ferric oxides: maghemite Q, γ-Fe_2O_3, hematite, α-Fe_2O_3, magnetite, Fe_3O_4.
5) Titanium oxides: anatase, TiO_2.
6) Phases with forsterite structure, Mg_2SiO_4.
7) Phases with kyanite structure, $Al_2(SiO_4)O)$.

The X-ray charts of the basalt samples tested at different temperatures are provided below.

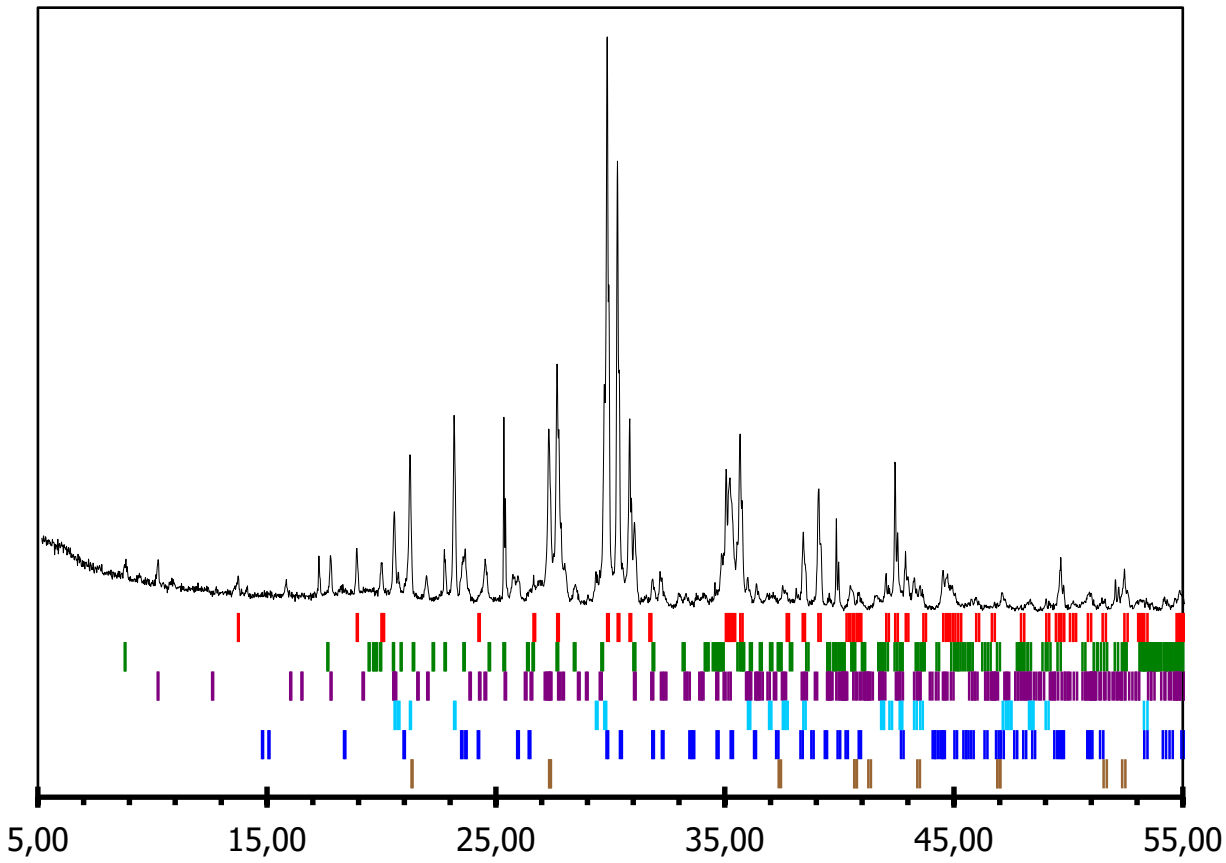

Fig. 5. X-ray chart of the initial basalt sample and the data of Rietveld quantitative phase analysis

Vertical lines indicate the location of reflex points for:

1. Augite, $(Mg,Ca,Fe)_2(SiO_3)_2$ (red),
2. Illite, $K(Al_4Si_2O_9(OH)_3$ (green),
3. Kaolinite 1A, $Al_2(Si_2O_5)(OH)_4$ (violet),
4. Tridymite O, SiO_2 (light blue),
5. Maghemite Q, □-Fe_2O_3 (blue),
6. Quartz Low, SiO_2 (brown).

Chart 3. Phase composition of examined samples

Initial basalt						
Augite *C*2/*c* grid	Illite *C*2/*c* grid	Kaolinite *P*1 grid	Tridymite $C222_1$ grid	Quartz $P3_121$ grid	Anatase $I4_1/a$ grid	Maghemite $P4_32_12$ grid
a = 9.7486 *b* = 8.8724 *c* = 5.2936 β = 106.00	*a* = 5.211 *b* = 9.113 *c* = 20.268 β = 95.76	*a* = 5.135 *b* = 8.645 *c* = 7.275 α = 91.98 β = 103.92 γ = 89.57	*a* = 8.621 *b* = 4.978 *c* = 8.355	*a* = 4.814 *c* = 5.274	*a* = 3.774 *c* = 9.520	*a* = 8.39 *c* = 8.13
63 %	**14 %**	**6 %**	**9 %**	**7 %**	**1 %**	**1 %**
1000°C, 1 h						
Augite *C*2/*c* grid	Illite *C*2/*c* grid	Kaolinite $\bar{P}1$ grid	Tridymite $C222_1$ grid			Magnetite *Fd*3*m* grid
a = 9.752 *b* = 8.874 *c* = 5.2971 β = 106.06	*a* = 5.179 *b* = 9.092 *c* = 20.297 β = 95.73	*a* = 5.147 *b* = 8.658 *c* = 7.191 α = 91.67 β = 104.06 γ = 89.69	*a* = 8.634 *b* = 4.992 *c* = 8.365			*a* = 8.391
55 %	**11 %**	**22 %**	**7 %**			**5 %**
1100°C, 1 h						
Augite *C*2/*c* grid			Cristobalite $P4_12_12$ grid	Forsterite *Pnma* grid	Kyanite $\bar{P}1$ grid	Magnetite *Fd*3*m* grid
a = 9.740 *b* = 8.865 *c* = 5.296 β = 106.05			*a* = 4.986 *c* = 6.901	*a* = 10.210 *b* = 5.972 *c* = 4.750	*a* = 7.077 *b* = 7.837 *c* = 5.562 α = 89.86 β = 100.77 γ = 105.75	*a* = 8.343
62 %			**2 %**	**10 %**	**22 %**	**3 %**
1200°C, 1 h						
Augite *C*2/*c* grid			Cristobalite $P4_12_12$ grid	Forsterite *Pnma* grid	Kyanite $\bar{P}1$ grid	Magnetite *Fd*3*m* grid
a = 9.7447 *b* = 8.8706 *c* = 5.2976 β = 106.12			*a* = 4.984 *c* = 6.916	*a* = 10.213 *b* = 5.979 *c* = 4.755	*a* = 7.076 *b* = 7.853 *c* = 5.588 α = 90.12 β = 100.85 γ = 105.72	*a* = 8.397
64 %			**2 %**	**11 %**	**13 %**	**11 %**

1300°C, 1 h						
					Hematite *R-3c* grid	Magnetite *Fd3m* grid
					a = 5.074 *c* = 14.34	*a* = 8.323
					5 %	**95 %**

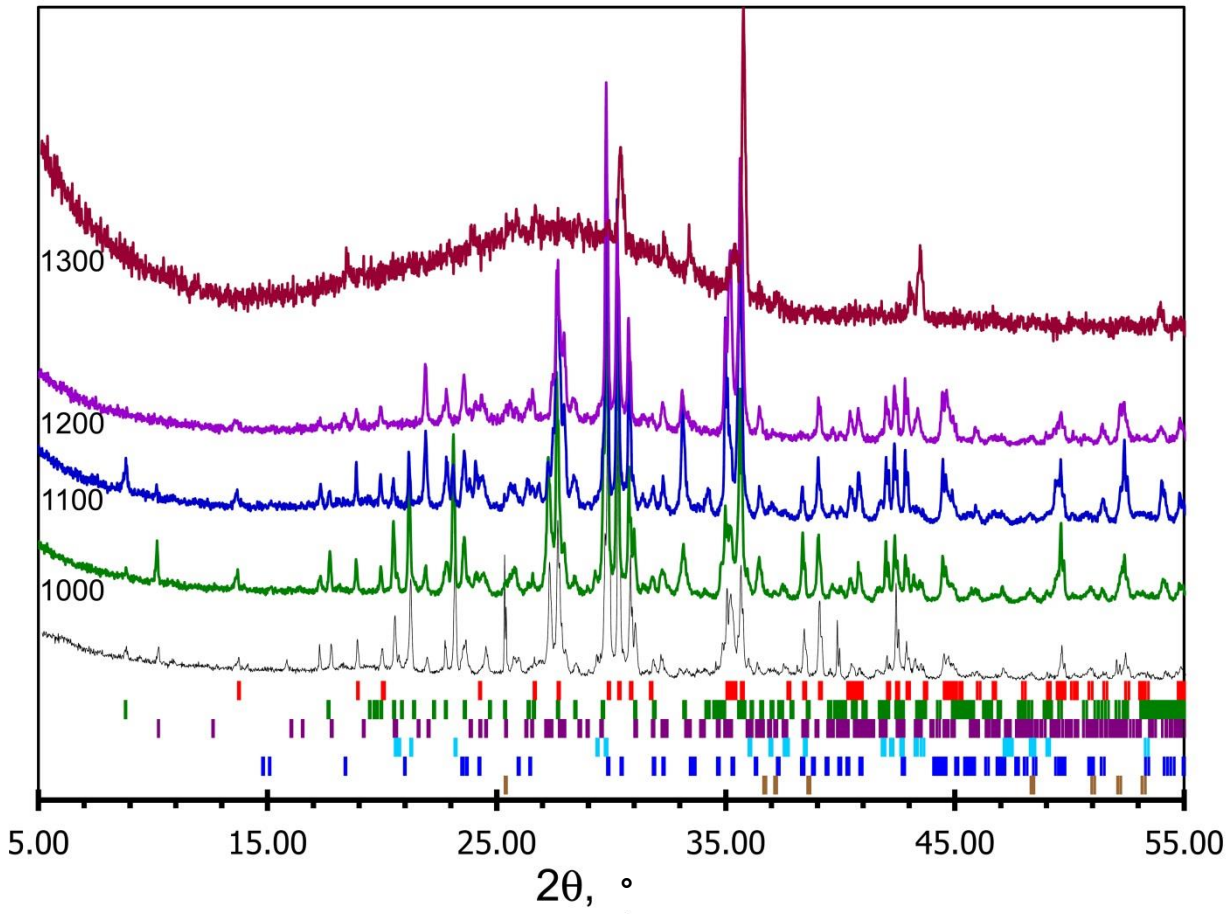

Fig. 6. X-ray diagram of the initial basalt sample (1) and of the samples annealed at the temperatures 1000-1300 °C

Vertical lines indicate the location of reflex points for:

1. Augite, $(Mg,Ca,Fe)_2(SiO_3)_2$ (red),
2. Illite, $K(Al_4Si_2O_9(OH)_3$ (green),
3. Kaolinite 1A, $Al_2(Si_2O_5)(OH)_4$ (purple),
4. Tridymite O, SiO_2 (light blue),
5. Maghemite Q, γ-Fe_2O_3 (blue),
6. Anatase, TiO_2 (brown).

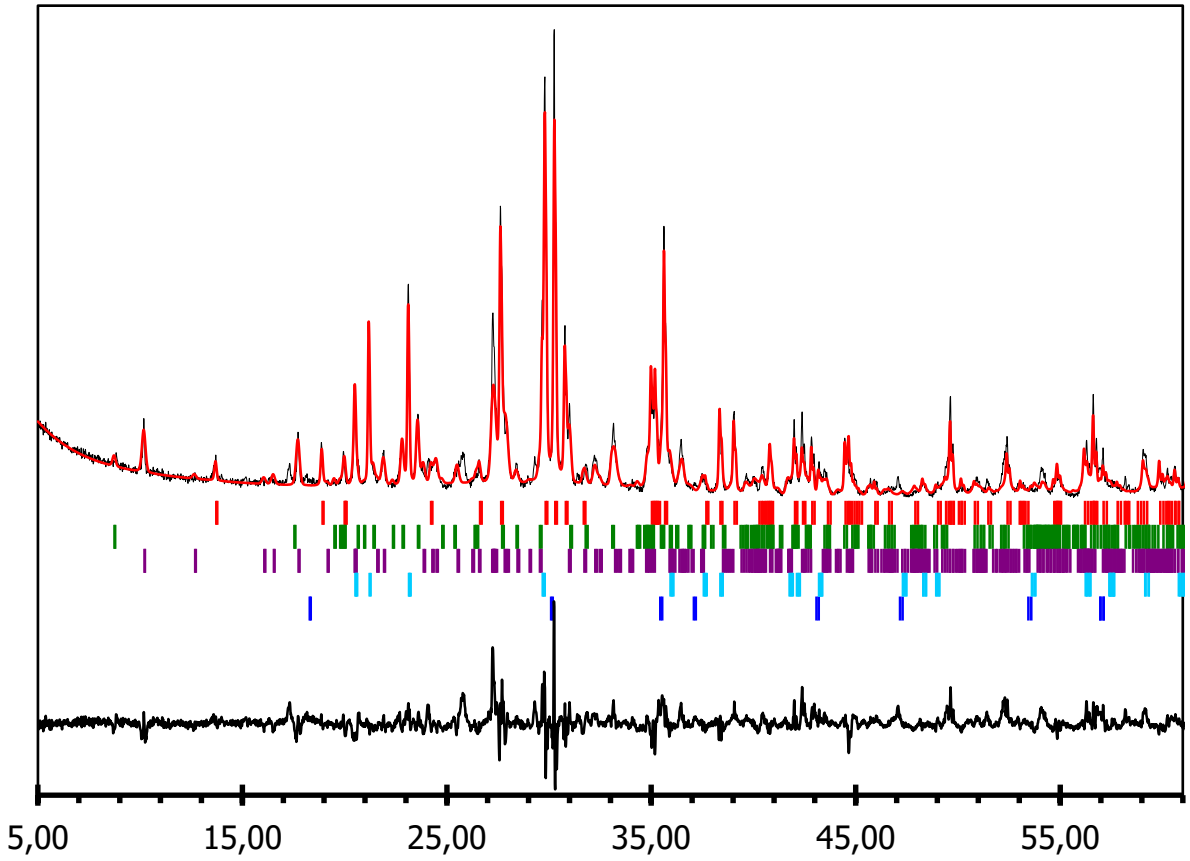

Fig. 7. X-ray chart of the initial basalt sample annealed at 1000°C for one hour and the data of Rietveld quantitative phase analysis

Experimental (black), calculated (red) and difference (below) charts. Vertical lines indicate the location of reflex points for:

1. Augite, $(Mg,Ca,Fe)_2(SiO_3)_2$ (red),
2. Illite, $K(Al_4Si_2O_9(OH)_3$ (green),
3. Kaolinite 1A, $Al_2(Si_2O_5)(OH)_4$ (purple),
4. Tridymite O, SiO_2 (light blue),
5. Magnetite, Fe_3O_4 (blue).

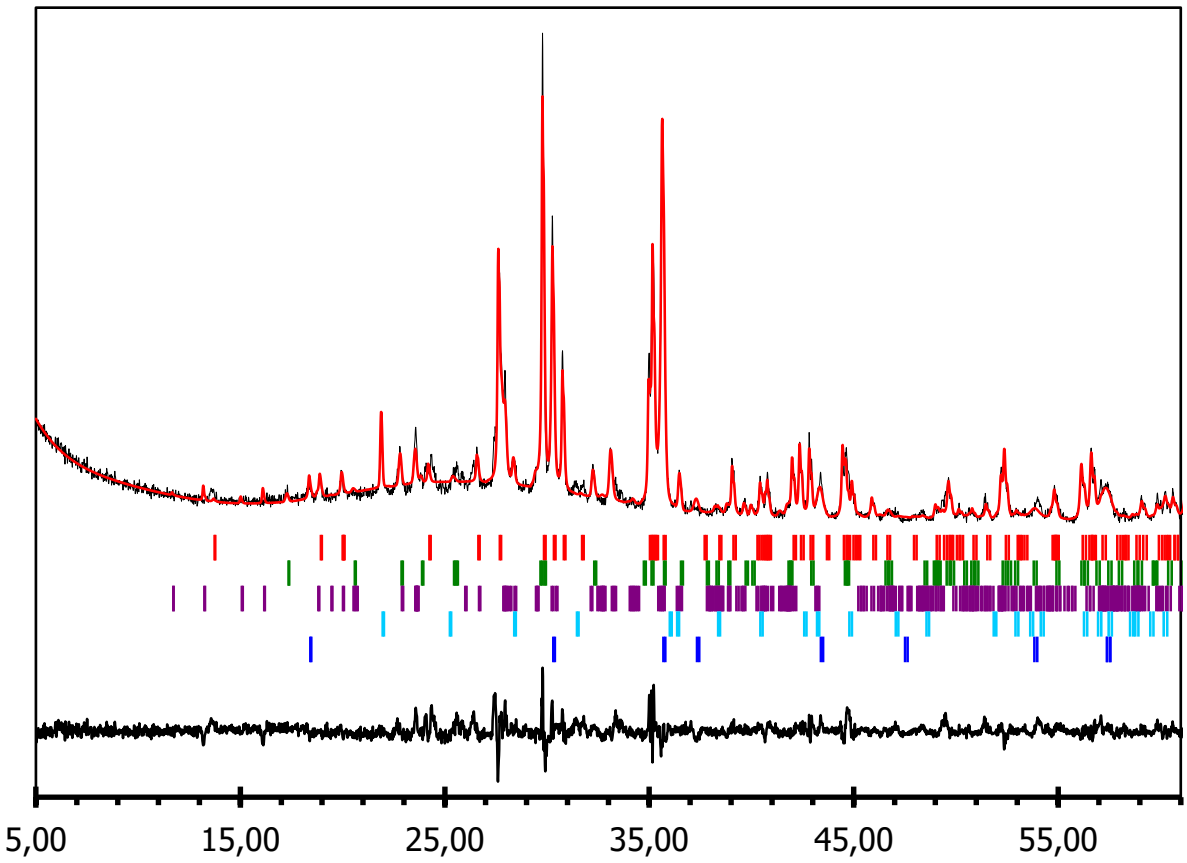

Fig. 8. X-ray chart of the initial basalt sample annealed at 1200°C for one hour and the data of Rietveld quantitative phase analysis

Experimental (black), calculated (red) and difference (below) charts. Vertical lines indicate the location of reflex points for:

1. Augite, $(Mg,Ca,Fe)_2(SiO_3)_2$ (red),
2. Forsterite, Mg_2SiO_4 (green),
3. Kyanite, $Al_2(SiO_4)O$ (purple),
4. Cristobalite low, SiO_2 (light blue),
5. Magnetite, Fe_3O_4 (blue).

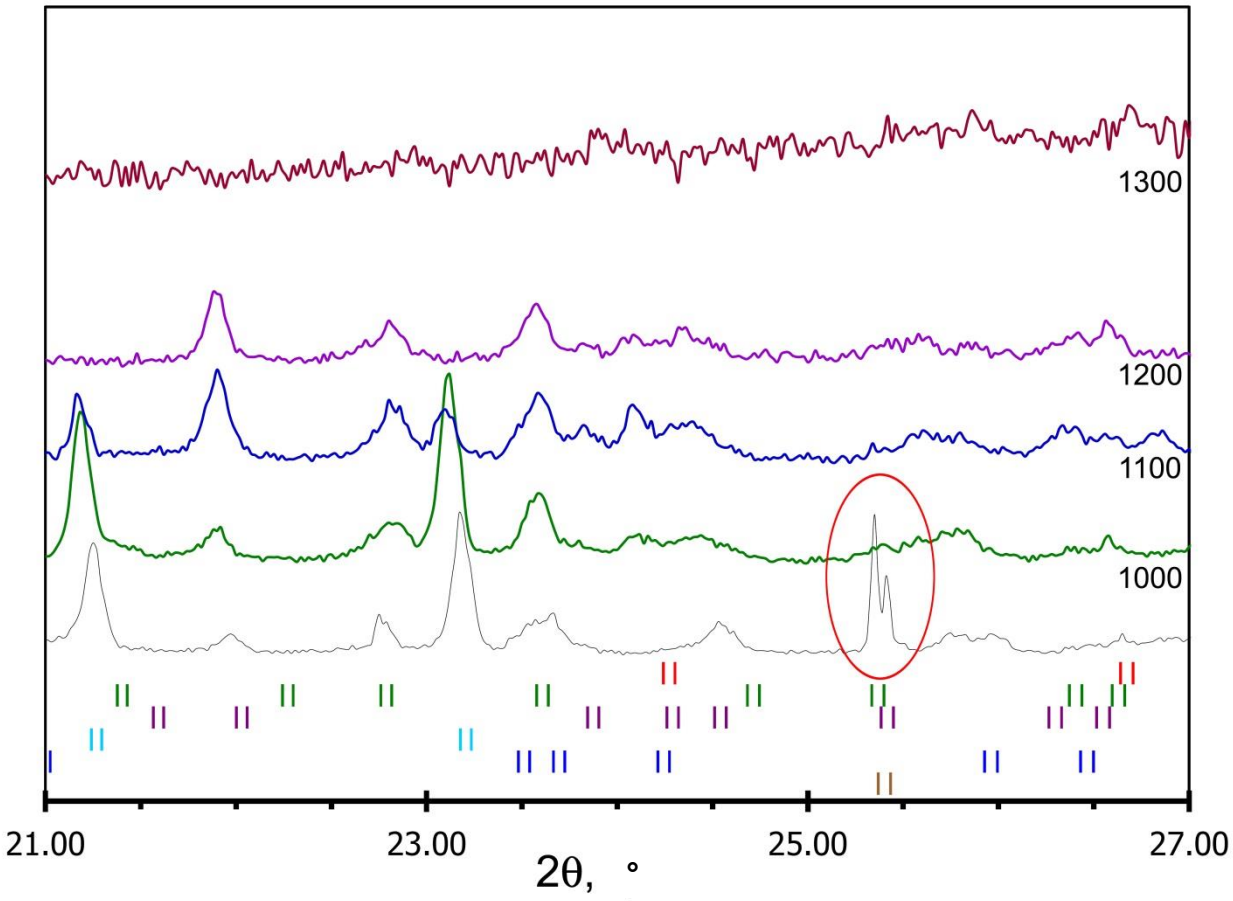

Fig. 9. X-ray charts of the initial basalt sample (1) and of the samples annealed at 1000-1300°C at the angles between 21° and 27° 2θ

Vertical lines indicate the location of reflex points for:

1. Augite, $(Mg,Ca,Fe)_2(SiO_3)_2$ (red),
2. Illite, $K(Al_4Si_2O_9(OH)_3$ (green),
3. Kaolinite 1A, $Al_2(Si_2O_5)(OH)_4$ (purple),
4. Tridymite O, SiO_2 (light blue),
5. Maghemite Q, γ-Fe_2O_3 (blue),
6. Anatase, TiO_{2pouj} (brown).

Annealing of the initial basalt sample leads already at 1000°C to the disappearance of anatase (TiO_2) reflexes highlighted by red ellipsis at Figure 10.

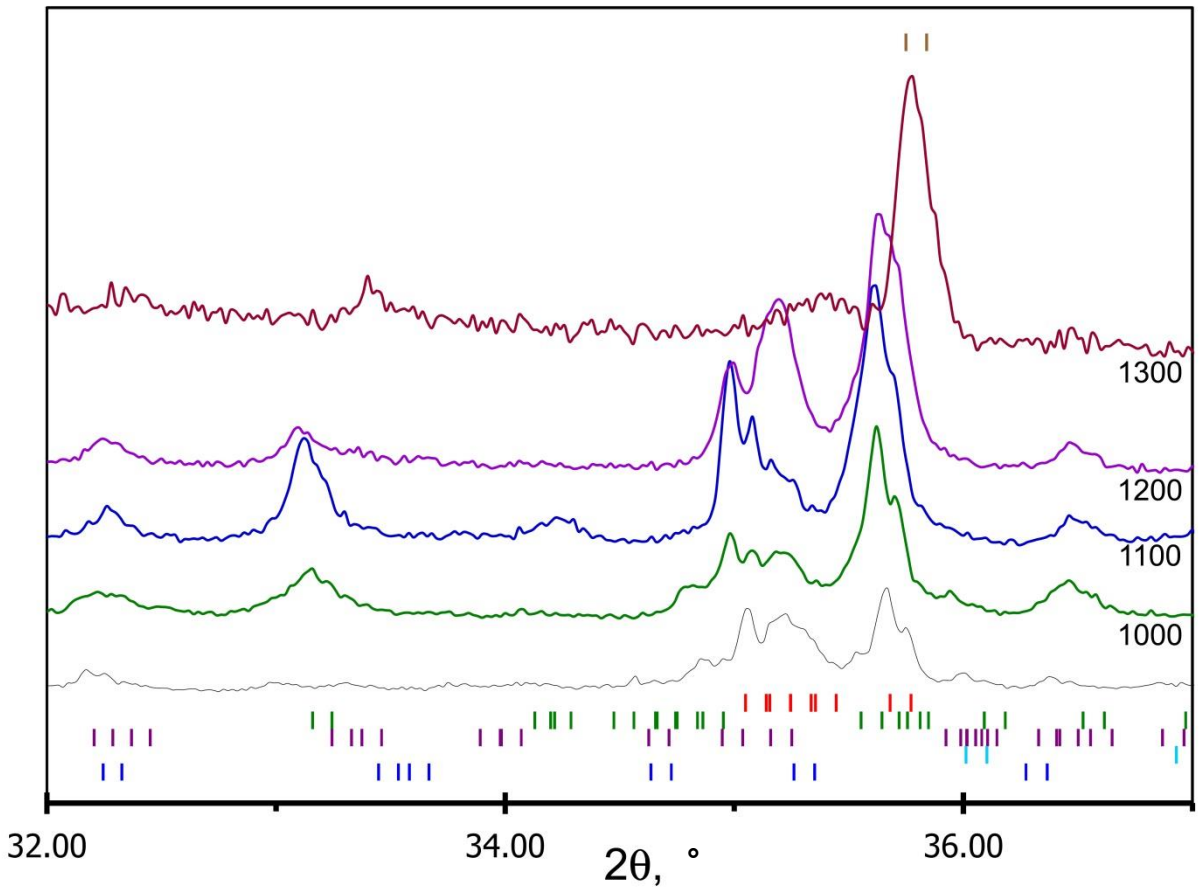

Fig. 10. X-ray charts of the initial basalt sample (1) and of the samples annealed at 1000-1300°C at the angles between 32°-37° 2θ

Vertical lines indicate the location of reflex points for:

1. Augite, $(Mg,Ca,Fe)_2(SiO_3)_2$ (red),
2. Illite, $K(Al_4Si_2O_9(OH)_3$ (green),
3. Kaolinite 1A, $Al_2(Si_2O_5)(OH)_4$ (purple),
4. Tridymite O, SiO_2 (light blue),
5. Maghemite Q, □-Fe_2O_3 (blue),
6. Magnetite, Fe_3O_4 (brown).

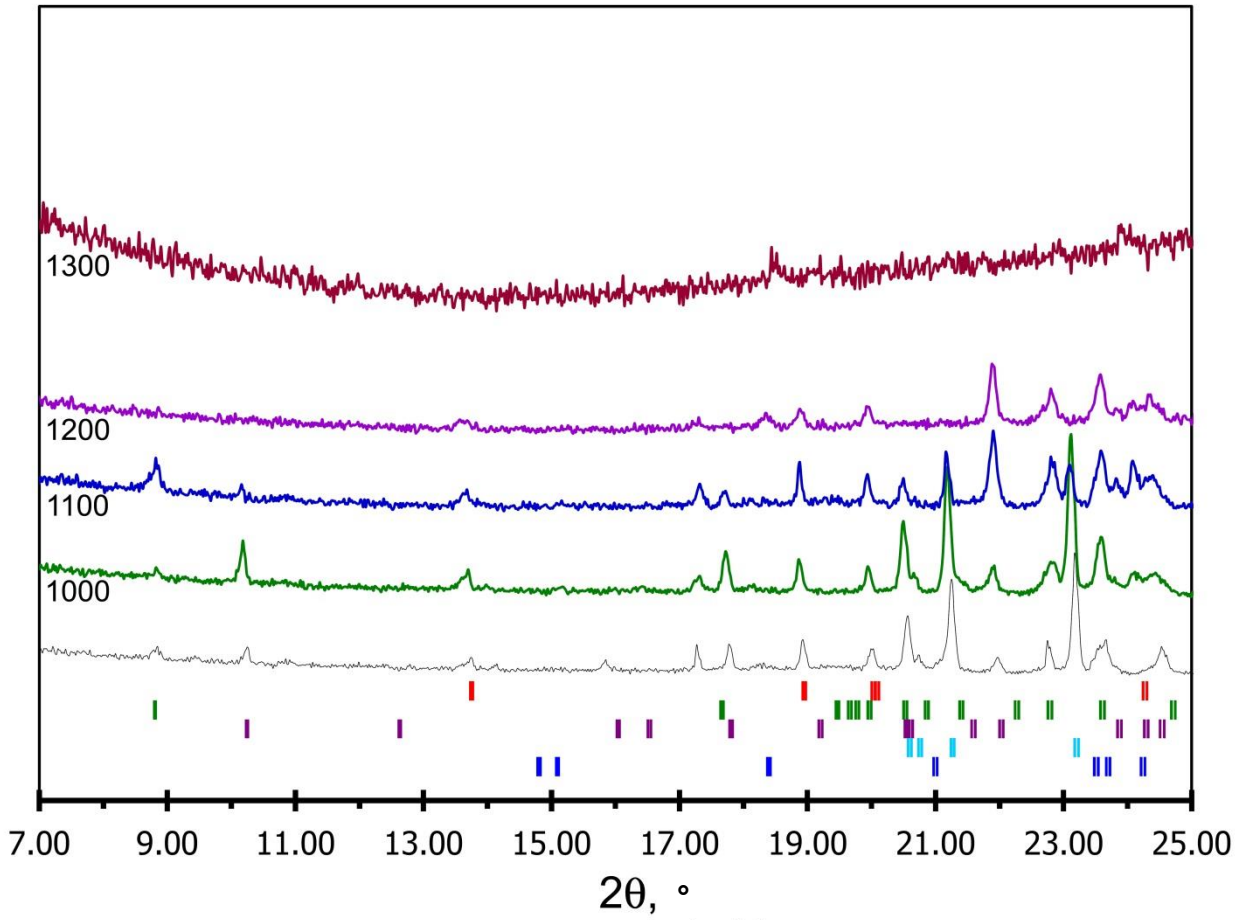

Fig. 11. X-ray charts of the initial basalt sample (1) and of the samples annealed at 1000-1300°C at the angles between 7°-25° 2θ

Vertical lines indicate the location of reflex points for:

1. Augite, $(Mg,Ca,Fe)_2(SiO_3)_2$ (red),
2. Illite, $K(Al_4Si_2O_9(OH)_3$ (green),
3. Kaolinite 1A, $Al_2(Si_2O_5)(OH)_4$ (purple),
4. Tridymite O, SiO_2 (light blue),
5. Maghemite Q, □-Fe_2O_3 (blue),
6. Anatase, TiO_2 (brown).

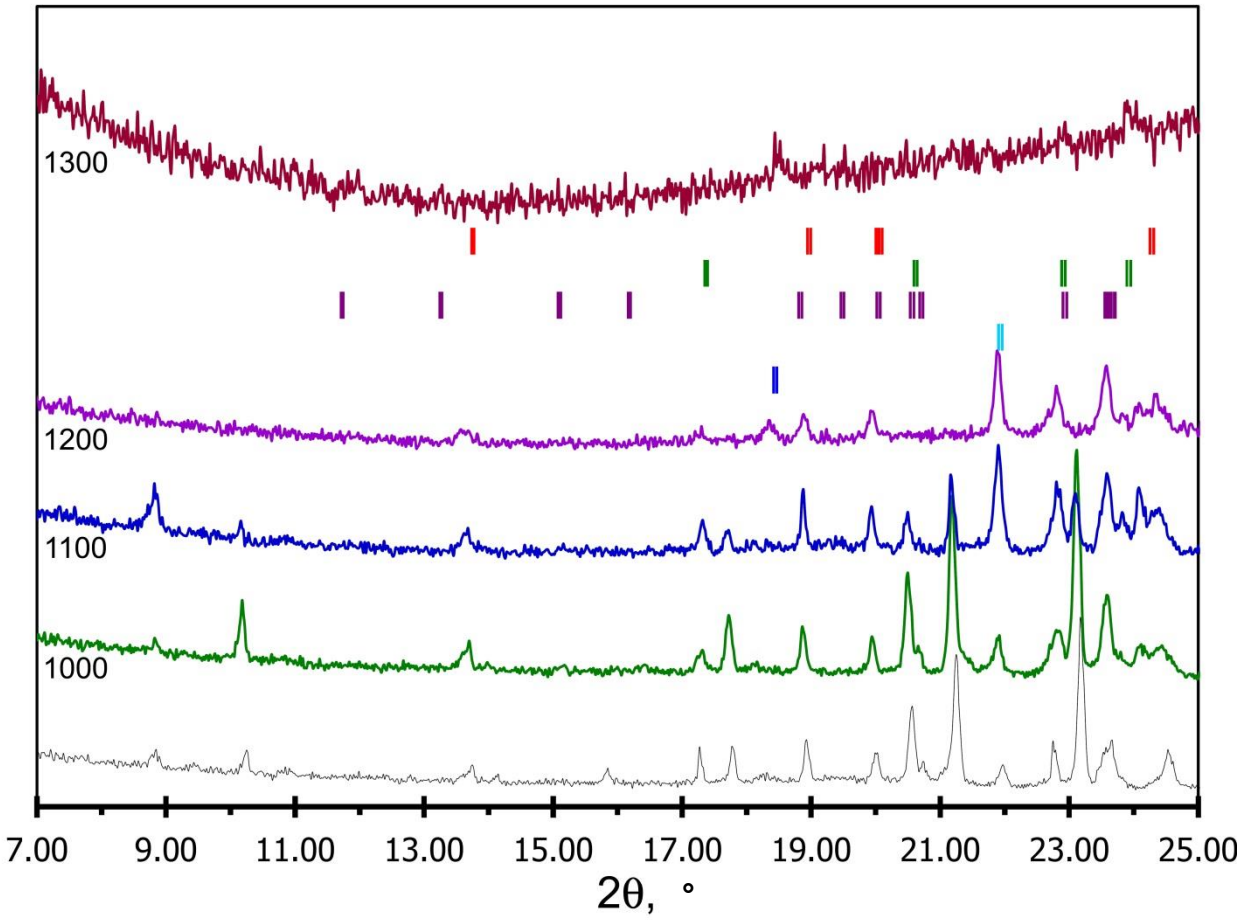

Fig. 12. X-ray charts of the initial basalt sample (1) and of the samples annealed at 1000-1300°C at the angles between 7°-25° 2θ

Vertical lines indicate the location of reflex points for:

1. Augite, $(Mg,Ca,Fe)_2(SiO_3)_2$ (red),
2. Forsterite, Mg_2SiO_4 (green),
3. Kyanite, $Al_2(SiO_4)O$ (purple),
4. Cristobalite low, SiO_2 (light blue),
5. Magnetite, Fe_3O_4 (blue).

The generalized data on the phase composition of the tested samples are provided in the Table 3. The evidence presented in Fig. 5 and Table 3 suggests the presence of 6 phases in initial basalt. These are: augite (63%) – basic phase, illite (14%), kaolinite (6%), tridymite and quartz, anatase and maghemite. Upon heating the initial sample up to 1000°C and keeping up the temperature for 1 hour, carbonates are decomposing and water is being discharged (Fig. 3, 4). The lines allocated to quartz and anatase are disappearing at X-ray charts. The share of augite lessens, and the share of kaolinite increases. The share of the magnetite-based phase increases as well. At 1000°C and above two new phases appear: forsterite and kyanite. It should be pointed out that the sample which has been processed at 1200°C for 1 hour contains

well-crystallized phases (Table 3). A visible halo of the glassy phase is missing on the chart. This is an indication that at 1200°C (1 h) only an insignificant part of basalt is being melted, although the melting temperature according to the DSC curve is 1176°C. Already at 1300°C (1 h) basalt rock is practically completely melted. No more than 5% of the crystalline phase (hematite and magnetite) are left. At subsequent work stages it should be cleared on which conditions the crystalline phase is being completely diluted or melted.

Annealing at 1200°C and higher temperatures leads to the formation of a magnetite-based phase (Fe_3O_4), the share of which increases according to the increase of annealing temperature (Picture 10, Table 3) and the formation of a hematite-based phase (α-Fe_2O_3) at the annealing temperature of 1300°C.

Annealing at the temperatures higher than 1100°C leads to the dissolution of illite reflexes ($K(Al_4Si_2O_9(OH)_3$, kaolinite 1A reflexes ($Al_2(Si_2O_5)(OH)_4$) and tridymite reflexes (O, SiO_2) as well as the development of silicates' reflexes with forsterite (Mg_2SiO_4) and kyanite ($Al_2(SiO_4)O$) reflexes (Table 3).

5. Definition of structural coordination state of iron cations

The change of oxidation degree and of the oxygen environment of iron cations within the samples in the process of heat treating was analysed using Moessbauer spectroscopy. Moessbauer spectra were obtained at the spectrometer of electrodynamic type with a multi-chambered analyzer. A ^{57}Co isotope located in a rhodium matrix was used as a γ-transmitter. Isomerous shifts were correlated with calibration spectrum α-Fe obtained at 298 K. Experimental spectra were approximated by the components of the Lorentzian shape using the UnivemMS software. Mole ration of iron cations was considered equal to their spectral contribution, assumed that the respective Debye-Waller factors differ insignificantly. The spectra of the initial and the heat-treated basalt are presented at the Figures 13-17, the data are summarized in Chart 4.

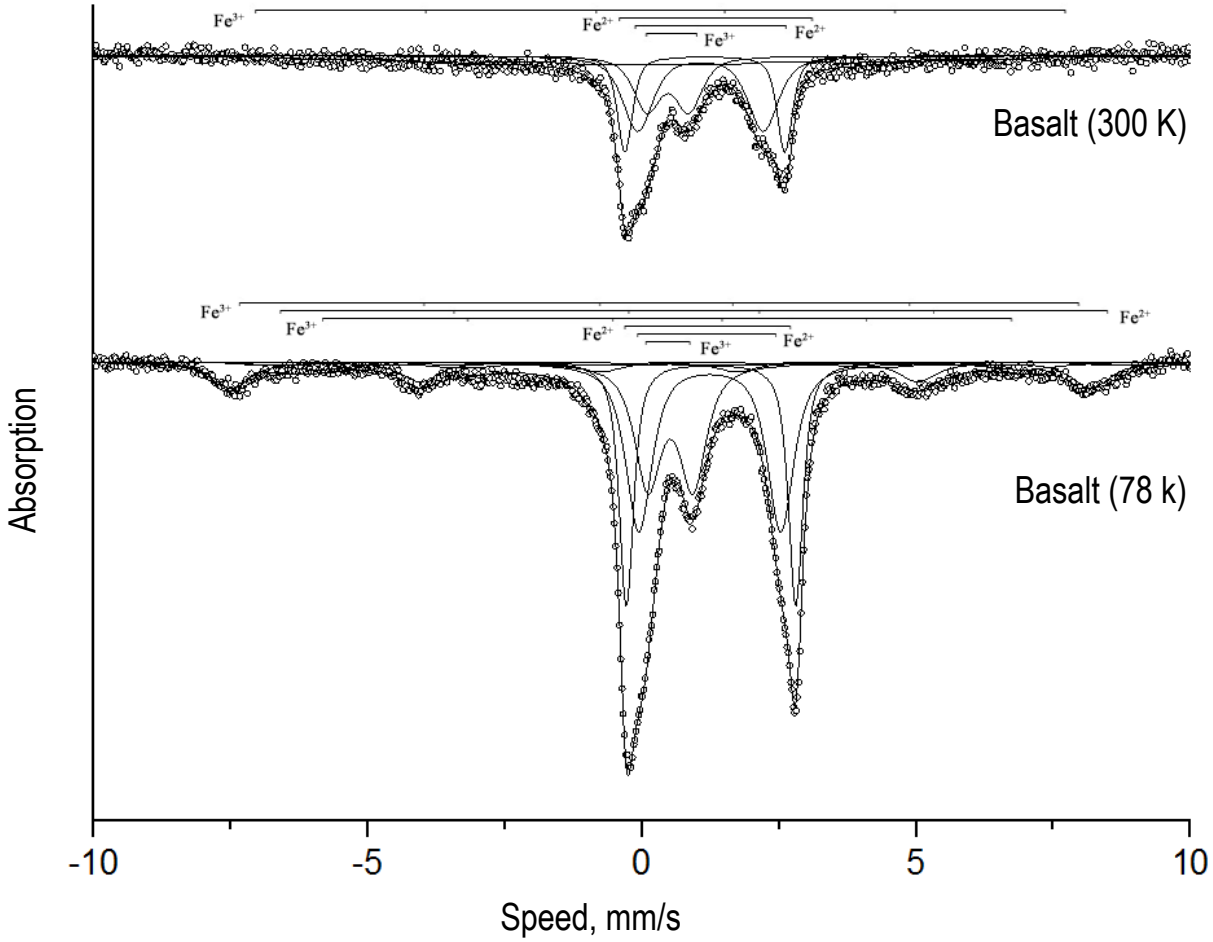

Fig. 13. Moessbauer spectra of the initial basalt mix

(the temperatures at which the spectra were obtained are indicated in brackets)

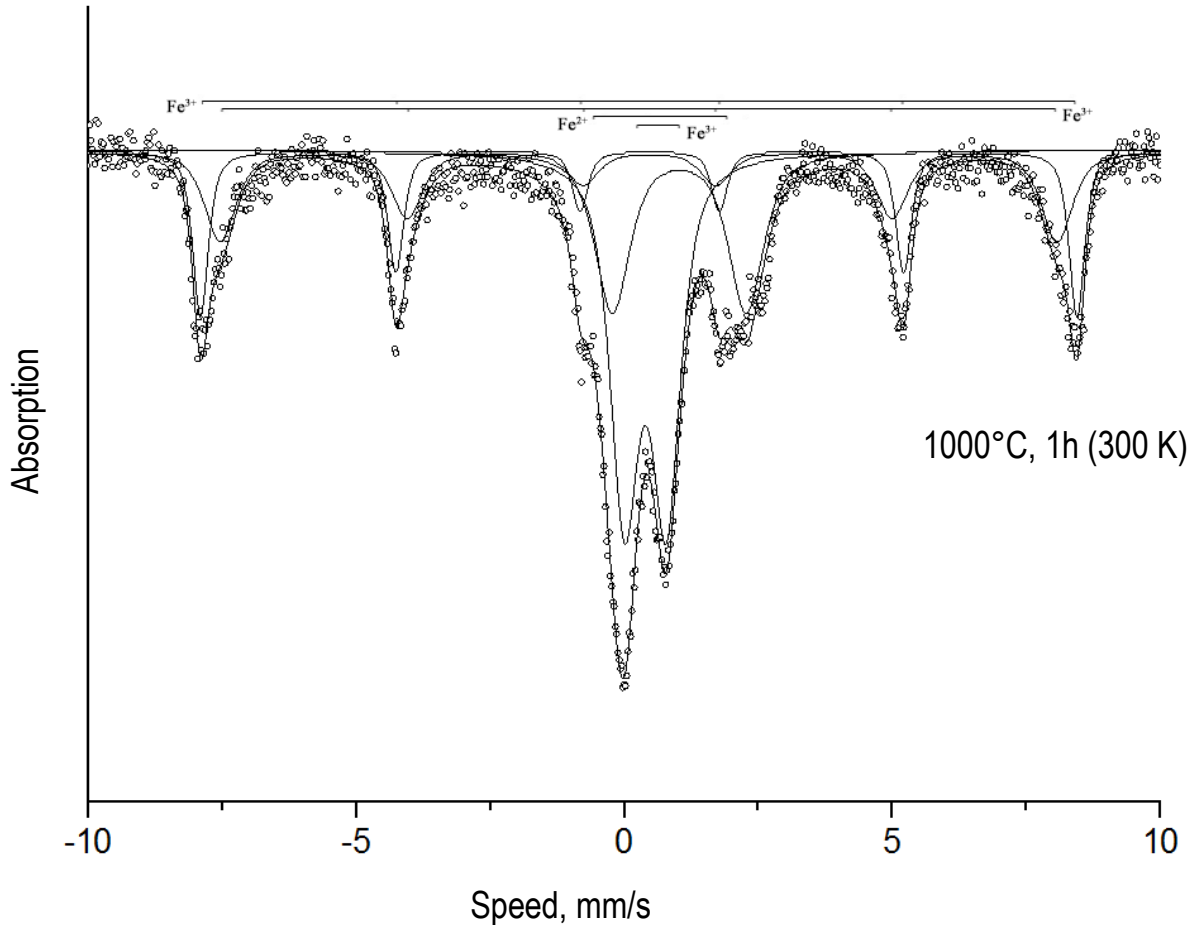

Fig. 14. Moessbauer spectra of air-hardened basalt at 1100 °C

(the temperatures at which the spectra were obtained are indicated in brackets)

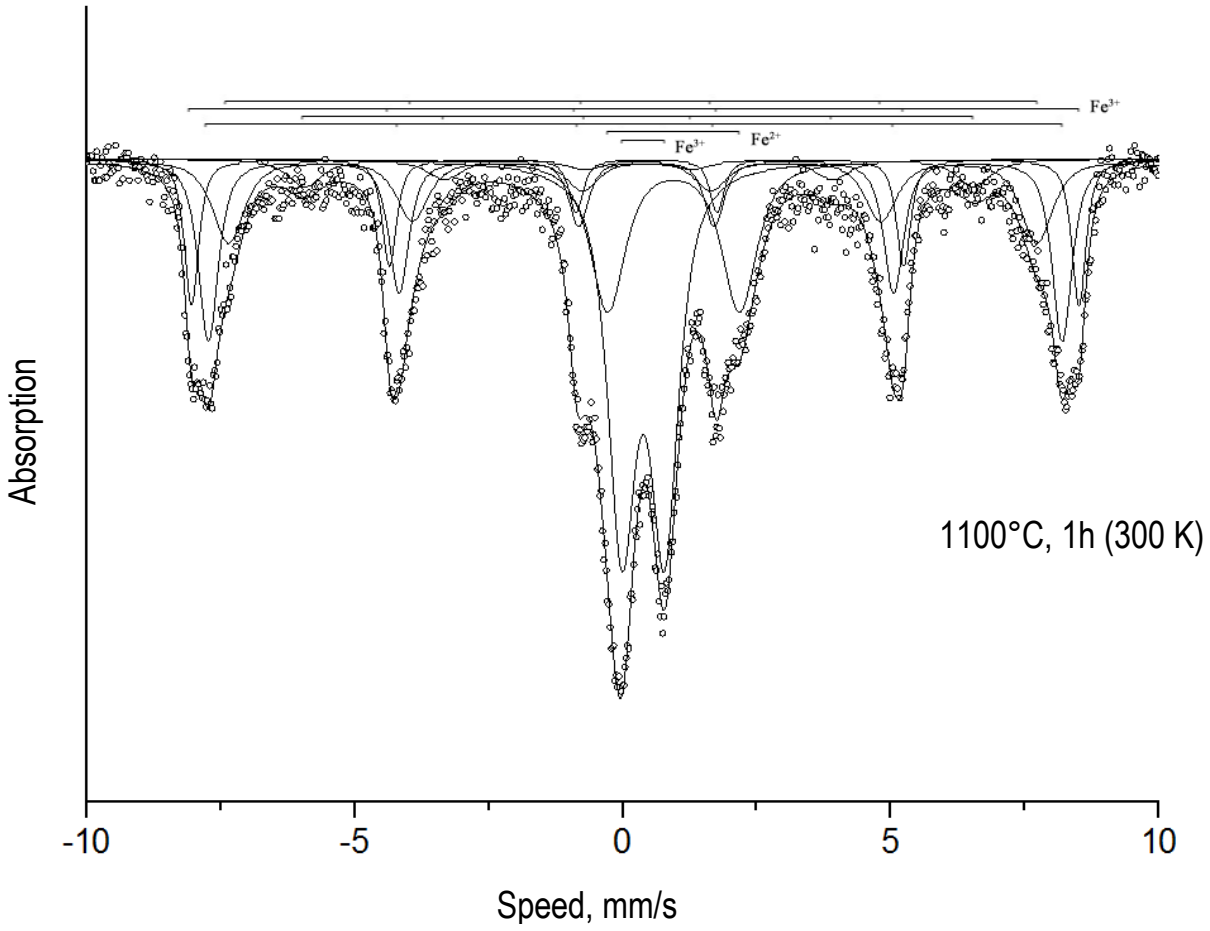

Fig. 15. Moessbauer spectra of air-hardened basalt at 1100 °C

(the temperatures at which the spectra were obtained are indicated in brackets)

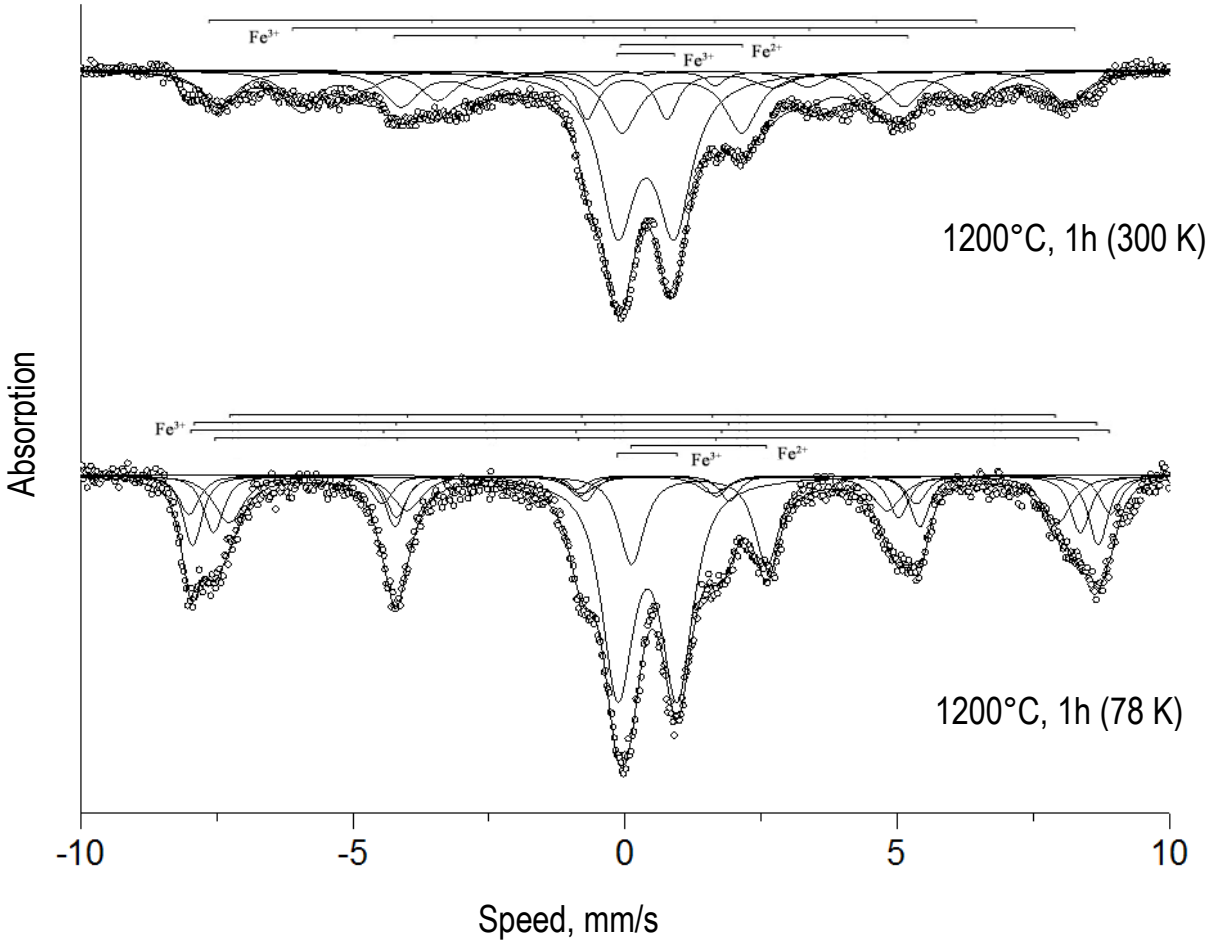

Fig. 16. Moessbauer spectra of air-hardened basalt at 1200 °C

(the temperatures at which the spectra were obtained are indicated in brackets)

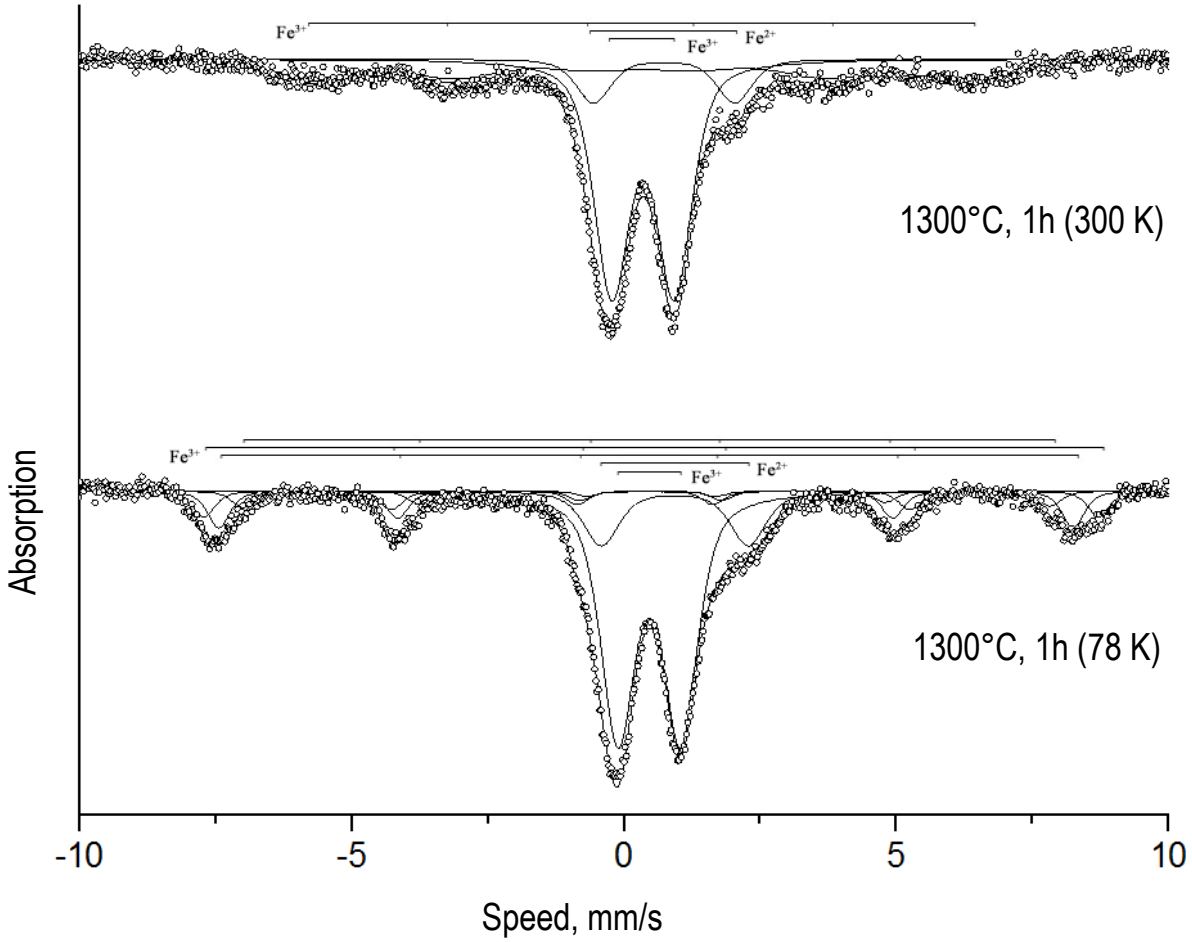

Fig. 17. Moessbauer spectra of air-hardened basalt at 1300 °C

(the temperatures at which the spectra were obtained are indicated in brackets)

Chart 3. Parameters of Moessbauer spectra of the initial basalt mix and of the mix annealed at the temperatures of 1000, 1100, 1200 и 1300°C

(δ – isomer shift referred to α-Fe; Δ - quadrupolar splitting; Γ – line width at half height; H – back margin; A – spectral contribution)

Sample	Components	δ	Δ	Γ	H	A
		±0.03 mm/sec			±2 kiloOersted	±5 %
Basalt (300 K)	Fe^{3+} (sextet)-1	0.30	0.00	1.51	381	23
	Fe^{2+}(doublet)-1	1.15	2.92	0.33	-	22
	Fe^{2+}(doublet)-2	1.07	2.29	0.66	-	33
	Fe^{3+}(doublet)-3	0.47	0.76	0.59	-	22
Basalt (78 K)	Fe^{3+}(sextet)-1	0.42	-0.14	0.76	486	13
	Fe^{2+}(sextet)-2	1.00	0.00	0.76	480	2
	Fe^{3+}(sextet)-3	0.50	0.00	1.99	400	9
	Fe^{2+}(doublet)-1	1.26	3.09	0.32	-	24
	Fe^{2+}(doublet)-2	1.24	2.59	0.57	-	30
	Fe^{3+}(doublet)-3	0.52	0.82	0.58	-	22
1000 °C, 1 h (300 K)	Fe^{3+}(sextet)-1	0.37	-0.21	0.35	508	20
	Fe^{3+}(sextet)-2	0.37	-0.20	0.69	485	22
	Fe^{2+}(doublet)-1	1.02	2.49	0.78	-	21
	Fe^{3+}(doublet)-1	0.39	0.78	0.64	-	37
1100 °C, 1 h (300 K)	Fe^{3+}(sextet)-1	0.32	-0.26	0.71	468	16
	Fe^{3+}(sextet)-2	0.34	-0.21	0.32	514	12
	Fe^{3+}(sextet)-3	0.29	0.02	0.78	387	5
	Fe^{3+}(sextet)-4	0.34	-0.21	0.44	494	22
	Fe^{2+}(doublet)-1	0.95	2.46	0.78	-	15
	Fe^{3+}(doublet)-2	0.38	0.79	0.62	-	30
1200 °C, 1 h (300 K)	Fe^{3+}(sextet)-1	0.01	-1.11	0.78	429	17
	Fe^{3+}(sextet)-2	0.19	1.82	0.78	437	13
	Fe^{3+}(sextet)-3	0.28	0.47	0.77	287	19
	Fe^{2+}(doublet)-1	1.05	2.20	0.74	-	14
	Fe^{3+}(doublet)-2	0.39	1.04	0.78	-	37
1200 °C, 1 h (78 K)	Fe^{3+}(sextet)-1	0.37	-0.08	0.65	473	16
	Fe^{3+}(sextet)-2	0.49	-0.22	0.42	517	14

	Fe^{3+}(sextet)-3	0.45	0.01	0.45	526	9
	Fe^{3+}(sextet)-4	0.41	-0.01	0.44	494	13
	Fe^{2+}(doublet)-1	1.37	2.49	0.55	-	12
	Fe^{3+}(doublet)-2	0.42	1.09	0.70	-	36
1300 °C, 1 h (300 K)	Fe^{3+}(sextet)-1	0.34	0.02	1.89	366	30
	Fe^{2+}(doublet)-1	0.73	2.59	0.77	-	12
	Fe^{3+}(doublet)-2	0.35	1.15	0.77	-	58
1300 °C, 1 h (78 K)	Fe^{3+}(sextet)-1	0.45	-0.09	0.49	461	5
	Fe^{3+}(sextet)-2	0.49	0.01	0.49	510	9
	Fe^{3+}(sextet)-3	0.39	0.01	0.49	487	12
	Fe^{2+}(doublet)-1	0.93	2.70	0.78	-	14
	Fe^{3+}(doublet)-2	0.46	1.15	0.75	-	60

The spectrum of the initial basalt mix is a superposition of the contributions of bi- and trivalent iron cations in a paramagnetic state with a correlation of Fe^{2+}/Fe^{3+} equal to 54:22. The spectra obtained at the temperature of liquid nitrogen are marked by the appearance of magnetic resolution (three sextets with internal field values of 486, 480 and 460 kiloOersted). The first sextet can be assigned to α- or γ-Fe_2O_3. The second sextet with an internal field value of 480 kiloOersted is close to Fe_3O_4. The third sextet, being a minor field component, is a sum of unresolved sextets of either Fe^{3+} or Fe^{2+}. The annealing of basalt at 1000 °C continued for 1 hour leads to the increase of magnetic-ordered iron ratio up to 42 %. The magnetic sextet in a Moessbauer spectrum with an internal field value of ~508 kiloOersted (T = 300 K) corresponds with a ferric hematite-like phase (Fe_2O_3); sextet with the inner field of ~485 kiloOersted corresponds with a partially substituted phase Fe_2O_3 with a non-magnetic cation, e.g. Al or Mg. The spectra of the samples annealed at 1100°C indicate the disintegration of sextets, which can be related to the formation of spinels, whereas iron is traceable in two positions, e.g. of magnetite (Fe_3O_4). The ratio of magnetic-ordered iron amounts to ~55 %. The increase of hardening temperature up to 1200°C leads to the change of state of iron cations. The value of a visible quadruple resolution close to zero can be related to the development of a ferrite-like phase, e.g. magnesium. The increase of hardening temperature up to 1300°C leads to the decrease of the magnetic-ordered iron. The noticeable broadening of spectral lines suggests the absence of a long-range order and a significant distortion of oxygen polyhedra coordinating the iron atoms. At a given temperature the correlation Fe^{2+}/Fe^{3+} is 14:60. The data of the spectrum in question allows to assume the presence of a spinel phase where iron can be included in tetrahedral as well as in octahedral structure. The sextet with an isomer shift of 0,45 mm/sec and an internal field of 461 kiloOersted corresponds with iron in an octahedral $^{VI}[Fe^{3+}]$ structure, whereas the sextets with isomer shifts of 0.49 and 0.39 mm/sec and internal magnetic fields of 510 and 487 kiloOersted correspond with iron cations in a tetrahedral $^{IV}[Fe^{3+}]$ structure.

6. Summary

1. The average chemical composition of the given basalt sample was defined. The composition data are compiled in Chart 1. It was shown that the chemical composition of the sample is substantially non-homogenous (see Chart 2 for data).
2. The melting temperature of the given basalt sample was defined (T = 1176^{o}C).
3. The quantitative and qualitative composition of phases comprising the given basalt sample were defined. It was demonstrated that the initial basalt consists of 6 phases (see Chart 3). The main phases are augite and illite.
4. It was observed that heat application changes the phase composition of initial basalt (see Chart 3). Below the temperature 1200^{o}C mainly crystalline phases exist. For complete melting a basalt sample has to be exposed to 1200^{o}C for a certain amount of time. The most resistant phases (phases with the highest melting temperature) are those based on iron compounds (magnetite and hematite). Their melting temperature exceeds 1300^{o}C. At 1300^{o}C hematite- and magnetite-based phases have been dtected in heat-strengthened glass.
5. The oxidation rate of iron ions, which play an important role in obtaining a homogenous (crystalline phase-free) melt of basalt rock, was defined. It was demonstrated that with increasing temperature the oxidation rate of iron ions was chaning from +2 to +3 (in general). The data of Moessbauer spectroscopy enabled a correct identification of the phases within the melt.